Pergamon

Int. J. Heat Mass Transfer. Vol. 38, No. 8, pp. 1467–1481, 1995

0017-9310/95 $9.50+0.00

0017-9310(94)00252-5

A new turbulence model for predicting fluid flow and heat transfer in separating and reattaching flows—II. Thermal field calculations

K. ABE and T. KONDOH

Toyota Central Research and Development Laboratories, Inc., Nagakute-cho, Aichi-gun, Aichi-ken 480-11, Japan

and

Y. NAGANO

Department of Mechanical Engineering, Nagoya Institute of Technology, Gokiso-cho, Showa-ku, Nagoya 466, Japan

(*Received* 24 *March* 1994 *and in final form* 8 *July* 1994)

Abstract—A new turbulence model to calculate complex turbulent heat transfer in separating and reattaching flows is proposed. This new model is a modified version of the latest low-Reynolds-number two-equation heat-transfer model, in which the main improvement is achieved by introducing the Kolmogorov velocity scale, $u_\varepsilon \equiv (\nu\varepsilon)^{1/4}$, instead of the friction velocity u_τ, to account for the near-wall and low-Reynolds-number effects in both attached and detached flows. After investigating the characteristics of various time scales for the heat-transfer model, we adopted a composite time scale which gives weight to a shorter scale among the velocity- and temperature-field time scales. It is validated that the present model predicts quite accurately the turbulent heat transfer in separating and reattaching flows downstream of a backward-facing step, which involve most of the essential physics of complex turbulent heat transfer, under various conditions of flow Reynolds number and upstream boundary-layer thickness. In addition, the computational results have revealed several new mechanistic features of the turbulent heat transfer in separating and reattaching flows.

1. INTRODUCTION

In many practical applications, flows accompany separation and subsequent reattachment. This flow detachment and reattachment almost always determines the key structure of the flow field and significantly influences the mechanism of heat transfer. For reliable evaluation of the turbulent heat-transfer coefficient in separating and reattaching flows, it is crucial to use turbulence models which can predict both the velocity and temperature fields with high accuracy.

So far, the k–ε model in combination with the assumption of a constant turbulent Prandtl number, Pr_t, has been frequently used to predict the heat transfer in separating and reattaching turbulent flows (see Launder [1]). For example, to grasp the essential physics of complex turbulent heat transfer in such flows, several attempts with this type of approach have been made to simulate the heat transfer downstream of a backward-facing step [2–4]. Though such an approach is useful, major problems remain: (1) In calculating the turbulent heat transfer by the k–ε model with a constant Pr_t, the wall functions are usually adopted as the boundary conditions. However, their application to recirculating flow regions is quite questionable. (2) The calculations with the previous k–ε models usually give 15–20% underprediction of the flow reattachment length in a backward-facing step flow [5, 6], although it is the most fundamental quantity to be predicted in separating and reattaching flows. (3) In situations where the similarity between the velocity and temperature fields does not hold, as in a boundary layer or a pipe flow subjected to a sudden change of the wall thermal condition [7, 8], Pr_t is far from constant in contrast to the situation in a simple boundary-layer flow where the velocity and the temperature fields develop simultaneously. Thus, for the accurate prediction of heat transfer in complex turbulent flows, we need to use turbulence models which fulfil the following requirements: (1) The flow fields can be simulated with sufficient accuracy. (2) The correct near-wall limiting behavior is reproduced for both the velocity and the temperature fields. (3) The assumption of constant Pr_t is avoided. (4) The temperature-field time scale is appropriately taken into account.

In an earlier paper [9], we proposed a new k–ε model for the application to flow fields with separation, which was modified from the low-Reynolds-number k–ε model of Nagano and Tagawa (hereinafter referred to as the NT model) [10]. The proposed model

NOMENCLATURE

A_{D1}, A_{D2}, A_λ, B_λ, C_λ, C_m constants in heat-transfer model functions
b_{ij} anisotropy tensor, $\overline{u_iu_j}/2k-\delta_{ij}/3$
C_f mean skin friction coefficient, $\tau_w/(\rho\bar{U}_0^2/2)$
C_f' fluctuating skin friction coefficient
C_{P1}, C_{P2}, C_{D1}, C_{D2} constants in transport equation for ε_t
C_μ, $C_{\varepsilon1}$, $C_{\varepsilon2}$ constants in velocity-field turbulence model
c_p specific heat at constant pressure
D channel width upstream of step
ER channel expansion ratio, $(D+H)/D$
$f_\mu, f_\varepsilon, f_d$ functions in velocity-field turbulence model
$f_{P1}, f_{P2}, f_{D1}, f_{D2}$ functions in temperature-field turbulence model
H height of backward-facing step
k turbulent kinetic energy, $\overline{u_iu_i}/2$
L_t turbulent length scale for heat transfer, $\alpha_t/k^{1/2}$
N_ξ, N_η numbers of grid points in ξ- and η-directions, respectively
n local coordinate normal to wall surface
$\bar{P}$ mean static pressure
Pr, Pr_t molecular and turbulent Prandtl numbers
q_w wall heat flux
R time-scale ratio, τ_t/τ_u
R_t turbulent Reynolds number, $k^2/\nu\varepsilon$
Re_H Reynolds number based on step height, $\bar{U}_0H/\nu$
Re_θ Reynolds number based on momentum thickness, $\bar{U}_0\theta/\nu$
St Stanton number, $q_w/[\rho c_p\bar{U}_0(\bar{T}_w-\bar{T}_0)]$
$\bar{T}$, t mean temperature and temperature fluctuation
$\bar{T}^+$ nondimensional mean temperature, $(\bar{T}_w-\bar{T})/t_\tau$
$\bar{T}_r$ reference temperature, $q_wH/(\rho c_p\alpha)$
$\overline{t^2}$ temperature variance
t_τ friction temperature, $q_w/(\rho c_pu_\tau)$
$\bar{U}$ mean velocity in x-direction
$\bar{U}_i$, u_i mean velocity and velocity fluctuation in i-direction
$\bar{U}^+$ nondimensional mean velocity, $\bar{U}/u_\tau$
u, v velocity fluctuations in x- and y-directions, respectively
u_ε Kolmogorov velocity scale, $(\nu\varepsilon)^{1/4}$
u_τ friction velocity, $\sqrt{|\tau_w|/\rho}$
X_R flow reattachment length
x Cartesian coordinate in streamwise direction with $x=0$ at step location
x_i Cartesian coordinate in i-direction
y Cartesian coordinate normal to streamwise direction with $y=0$ at step bottom
y^+ nondimensional distance from wall surface, $u_\tau y/\nu$
y^* nondimensional distance from wall surface, $u_\varepsilon y/\nu$
$D/D\tau$ substantial derivative, $\partial/\partial\tau+\bar{U}_j\partial/\partial x_j$
$\overline{(\,)}$ ensemble-averaged values.

Greek symbols

α, α_t molecular and eddy diffusivities for heat
δ 99% boundary layer thickness
δ_{ij} Kronecker delta
ε dissipation rate of turbulent kinetic energy, $\nu\overline{(\partial u_i/\partial x_j)(\partial u_i/\partial x_j)}$
ε_t dissipation rate of $\overline{t^2}/2$, $\alpha\overline{(\partial t/\partial x_j)(\partial t/\partial x_j)}$
ξ generalized coordinate in inlet-to-outlet direction
η generalized coordinate in lower to upper wall direction
θ momentum thickness
κ Von Kármán's universal constant
ν, ν_t kinematic viscosity and eddy viscosity
ρ density
σ_k, σ_ε, σ_h, σ_ϕ model constants for turbulent diffusion of k, ε, $\overline{t^2}$ and ε_t
τ time
τ_m characteristic time scale for turbulent heat transfer
τ_u, τ_t time scales of velocity and temperature fields, k/ε, $\overline{t^2}/2\varepsilon_t$
τ_w wall shear stress.

Subscripts

e outer edge of boundary layer
i, j 1 and 2 denote x- and y-directions, respectively
max maximum value on step side wall
max(x) maximum value at a location x
n normal direction from wall surface
R flow reattachment point
w wall surface
0 reference value at inlet position ($x=-3.8H$) of back-step channel.

can reproduce the near-wall limiting behavior as correctly as the original one [9]. In addition, the accuracy in calculating separating and reattaching flows downstream of a backward-facing step has been dramatically improved with this new model. In particular, the calculated flow reattachment lengths were in excellent agreement with the measurements for a variety of experimental conditions [9].

Over the last several years, two-equation heat-transfer models have made rapid progress [11–13], leading to substantial improvements in the accuracy of the heat-transfer prediction in complex turbulent flows. Among the existing two-equation heat-transfer models, the model developed by Nagano *et al.* (hereinafter referred to as the NTT model) [12] is regarded as one of the most reliable. The NTT model can correctly reproduce the near-wall limiting behavior of scalar turbulence quantities for any wall thermal conditions, and provides accurate predictions for the attached flow heat transfer [12, 13]. However, since the model functions of the NTT model contain the friction velocity u_τ, it breaks down around the separating and the reattaching points where $u_\tau = 0$. As a result, contrary to the real phenomena, the NTT model forces the turbulent heat flux to vanish there.

In this study, we propose a new two-equation heat-transfer model, based on the modification of the NTT model [12, 13]. The principal improvement is made using the Kolmogorov velocity scale $u_\varepsilon \equiv (\nu\varepsilon)^{1/4}$ instead of the friction velocity u_τ to account for the near-wall and low-Reynolds-number effects. As discussed in the preceding paper [9], the velocity scale u_ε vanishes at neither the separating nor the reattaching points in contrast to the friction velocity u_τ. Besides this major modification, we have examined in detail what type of hybrid time scale is best suited to the characteristic time scale for turbulent heat transfer under complex thermal conditions.

The calculations show that the new model is capable of predicting the heat transfer in separating and reattaching flows downstream of a backward-facing step quite successfully. The calculated distribution of the Stanton number, which is the most important quantity in heat transfer, is in almost perfect agreement with experiments under various conditions of the Reynolds number and the upstream boundary-layer thickness. Furthermore, from the present computational results, we have elucidated how the flow-field structures affect the heat-transfer mechanism in separating and reattaching flows.

2. TWO-EQUATION MODEL FOR VELOCITY FIELD

A velocity field is described with the following governing equations based on the eddy-viscosity approximation [9, 10]:

$$\frac{\partial \bar{U}_i}{\partial x_i} = 0 \tag{1}$$

$$\frac{D\bar{U}_i}{D\tau} = -\frac{1}{\rho}\frac{\partial \bar{P}}{\partial x_i} + \frac{\partial}{\partial x_j}\left\{\nu\left(\frac{\partial \bar{U}_i}{\partial x_j} + \frac{\partial \bar{U}_j}{\partial x_i}\right) - \overline{u_i u_j}\right\} \tag{2}$$

$$\frac{Dk}{D\tau} = \frac{\partial}{\partial x_j}\left\{\left(\nu + \frac{\nu_t}{\sigma_k}\right)\frac{\partial k}{\partial x_j}\right\} - \overline{u_i u_j}\frac{\partial \bar{U}_i}{\partial x_j} - \varepsilon \tag{3}$$

$$\frac{D\varepsilon}{D\tau} = \frac{\partial}{\partial x_j}\left\{\left(\nu + \frac{\nu_t}{\sigma_\varepsilon}\right)\frac{\partial \varepsilon}{\partial x_j}\right\} - C_{\varepsilon 1}\frac{\varepsilon}{k}\overline{u_i u_j}\frac{\partial \bar{U}_i}{\partial x_j} - C_{\varepsilon 2} f_\varepsilon \frac{\varepsilon^2}{k} \tag{4}$$

with

$$-\overline{u_i u_j} = \nu_t\left(\frac{\partial \bar{U}_i}{\partial x_j} + \frac{\partial \bar{U}_j}{\partial x_i}\right) - \frac{2}{3}k\delta_{ij}. \tag{5}$$

In equations (3) and (4), f_ε is the model function, and $C_{\varepsilon 1}$, $C_{\varepsilon 2}$, σ_k and σ_ε are the model constants.

In modeling the eddy viscosity, ν_t, in equation (5), it is necessary to employ a turbulent length scale which works appropriately in both the regions away from and close to the wall [10, 14]. In our preceding paper [9], we proposed the following formula for ν_t:

$$\nu_t = C_\mu\left\{\frac{k^2}{\varepsilon} + 5k^{1/2}\left(\frac{\nu^3}{\varepsilon}\right)^{1/4} f_d\right\}\left\{1 - \exp\left(-\frac{y^*}{14}\right)\right\}^2 \tag{6}$$

where $y^* = u_\varepsilon y/\nu$. In equation (6), f_d is the model function introduced to accord consistently with the standard k–ε model formulation of $\nu_t = C_\mu k^2/\varepsilon$ away from the wall, i.e. $f_d = \exp\{-(R_t/200)^2\}$. Equation (6) can be rewritten in the conventional form as follows [9]:

$$\nu_t = C_\mu f_\mu \frac{k^2}{\varepsilon} \tag{7}$$

where

$$f_\mu = \left\{1 - \exp\left(-\frac{y^*}{14}\right)\right\}^2\left[1 + \frac{5}{R_t^{3/4}}\exp\left\{-\left(\frac{R_t}{200}\right)^2\right\}\right]. \tag{8}$$

The other model function and the model constants used in the present modified k–ε model are as follows [9]:

$$f_\varepsilon = \left\{1 - \exp\left(-\frac{y^*}{3.1}\right)\right\}^2 \times\left[1 - 0.3\exp\left\{-\left(\frac{R_t}{6.5}\right)^2\right\}\right] \tag{9}$$

$C_\mu = 0.09$, $\sigma_k = 1.4$, $\sigma_\varepsilon = 1.4$, $C_{\varepsilon 1} = 1.5$, $C_{\varepsilon 2} = 1.9$.

The most important feature of the present k–ε model is the introduction of the Kolmogorov velocity scale, $u_\varepsilon = (\nu\varepsilon)^{1/4}$, instead of the friction velocity u_τ, to account for the near-wall and low-Reynolds-number effects in both attached and detached flows [9]. This model can reproduce the correct near-wall asymptotic relations of turbulence, i.e. $k \propto y^2$, $\varepsilon \propto y^0$, $\nu_t \propto y^3$ and $-\overline{uv} \propto y^3$ for $y \to 0$.

3. TWO-EQUATION MODEL FOR THERMAL FIELD

3.1. *Governing equations*

A thermal field can be described with the following governing equations by introducing the eddy diffusivity for heat, α_t:

$$\frac{D\bar{T}}{D\tau} = \frac{\partial}{\partial x_j}\left(\alpha\frac{\partial \bar{T}}{\partial x_j} - \overline{u_j t}\right) \tag{10}$$

$$\frac{D\overline{t^2}}{D\tau} = \frac{\partial}{\partial x_j}\left\{\left(\alpha + \frac{\alpha_t}{\sigma_h}\right)\frac{\partial \overline{t^2}}{\partial x_j}\right\} - 2\overline{u_j t}\frac{\partial \bar{T}}{\partial x_j} - 2\varepsilon_t \tag{11}$$

$$\frac{D\varepsilon_t}{D\tau} = \frac{\partial}{\partial x_j}\left\{\left(\alpha + \frac{\alpha_t}{\sigma_\phi}\right)\frac{\partial \varepsilon_t}{\partial x_j}\right\} - C_{P1}f_{P1}\frac{\varepsilon_t}{\overline{t^2}}\overline{u_j t}\frac{\partial \bar{T}}{\partial x_j}$$

$$- C_{P2}f_{P2}\frac{\varepsilon_t}{k}\overline{u_i u_j}\frac{\partial \bar{U}_i}{\partial x_j} - C_{D1}f_{D1}\frac{\varepsilon_t^2}{\overline{t^2}} - C_{D2}f_{D2}\frac{\varepsilon\varepsilon_t}{k} \tag{12}$$

where

$$-\overline{u_j t} = \alpha_t\frac{\partial \bar{T}}{\partial x_j}. \tag{13}$$

In equations (11) and (12), f_{P1}, f_{P2}, f_{D1}, f_{D2} are the model functions and C_{P1}, C_{P2}, C_{D1}, C_{D2}, σ_h and σ_ϕ are the model constants as discussed below.

3.2. *Modeling eddy diffusivity for heat*

In modeling α_t in equation (13), we need to adopt an appropriate turbulent length scale characterizing the turbulent heat transport in both the regions away from and close to the wall, as in the modeling of a velocity field [10, 14]. Furthermore, it is extremely important in modeling α_t to take into account the relation between the velocity- and temperature-field time scales [11–13].

First, we consider how the time scales should be incorporated in modeling α_t. The eddy diffusivity for heat in the two-equation heat-transfer model can be generally expressed as follows:

$$\alpha_t \propto k\tau_m = k^{1/2}(k^{1/2}\tau_m) \tag{14}$$

where τ_m is the composite (hybrid) time scale characterizing turbulent heat transfer which depends on both the velocity-field time scale, $\tau_u = k/\varepsilon$, and the temperature-field time scale, $\tau_t = \overline{t^2}/2\varepsilon_t$. Equation (14) indicates that α_t consists of the turbulent velocity scale, $k^{1/2}$, and the turbulent length scale, $(k^{1/2}\tau_m)$. The composite time scale, τ_m, proposed in the previous studies [11, 12, 15] can be described with the following generalized formula:

$$\tau_m \propto (\tau_u^l \tau_t^m) = \tau_u R^m \quad (l+m=1) \tag{15}$$

where $R = \tau_t/\tau_u$ is the time-scale ratio. Note that this type of hybrid time scale is also used in a turbulent heat-flux model (e.g. see Elghobashi and Launder [16]), and there are several choices in the combination of l and m. Zeman and Lumley [17], on the other hand, introduced the following composite time scale in modeling a buoyancy-driven mixed layer:

$$\tau_m \propto (1/\tau_u + C_m/\tau_t)^{-1} = \tau_u\{R/(C_m+R)\} \tag{16}$$

where C_m is a constant. The composite time scale defined by equation (16) is the harmonic average of the velocity- and temperature-field time scales. This suggests that the shorter time scale among τ_u and τ_t is more important for turbulent heat transfer. Note that this type of hybrid time scale has been adopted in a recent turbulent heat-flux model [18]. In the present study, we construct two-equation heat-transfer models based on three kinds of time scales given by equation (15) with different m and equation (16).

On the other hand, we should appropriately introduce a model function in α_t to account for wall-proximity effects. Generalizing the formula for α_t in the NTT model [12], α_t can be expressed as follows, based on equation (14), except in immediate proximity to the wall surface:

$$\alpha_t \propto k\tau_m\left\{1-\exp\left(-\frac{y^*}{A_\lambda}\right)\right\}\left\{1-\exp\left(-\frac{y^*}{B_\lambda}\right)\right\}. \tag{17}$$

Here, we have adopted y^* instead of y^+ for the model application to separating and reattaching flows. We have determined the constants A_λ and B_λ with reference to Cebeci's discussion [19], i.e. $A_\lambda = 14$, which is the same as in equation (6), and $B_\lambda = 14/Pr^{1/2}$.

In close proximity to the wall, the conservation of the temperature variance [equation (11)] is maintained by dissipating almost all $\overline{t^2}$ diffused from the region away from the wall, which is the same mechanism as in the velocity field [10, 20]. Therefore, it is appropriate to adopt a high-wavenumber-range scale dominating the dissipation process in modeling α_t close to the wall. Considering that the ratio between the temperature- and velocity-field time scales for dissipative motions is represented by $(R/Pr)^{1/2}$ [18], the eddy diffusivity for heat in proximity to the wall can be expressed as follows:

$$\alpha_t \propto \nu_t(R/Pr)^{1/2}. \tag{18}$$

The eddy diffusivity for heat given by equation (18) has exactly the same functional dependency of the time-scale ratio R as in the NTT model, so that this representation for α_t can reproduce the near-wall asymptotic relations correctly in both cases with and without the temperature fluctuations on the wall surface [12, 13].

Thus, we propose the following expression for the eddy diffusivity for heat using the characteristic time scale defined by equation (16) (hereinafter referred to as model A):

$$\alpha_t = C_\lambda\left\{\frac{k^2}{\varepsilon}\left(\frac{2R}{C_m+R}\right) + 3k^{1/2}\left(\frac{\nu^3}{\varepsilon}\right)^{1/4}\frac{(2R)^{1/2}}{Pr}f_d\right\}$$

$$\times\left\{1-\exp\left(-\frac{y^*}{14}\right)\right\}\left\{1-\exp\left(-\frac{Pr^{1/2}y^*}{14}\right)\right\}. \tag{19}$$

Here, we put $C_m = 0.5$ so that the resultant turbulent Prandtl number Pr_t $(= \nu_t/\alpha_t)$ may be equal to a stan-

dard value of 0.9 when values of C_λ and R are set to $C_\lambda = 0.1$ as in the NTT model [12] and $R = 0.5$, as is commonly assumed in an equilibrium boundary-layer heat transfer. We also examine two formulae for α_t based on equation (15) for comparison. The first is the representation with $m = 1$ (hereinafter referred to as model B):

$$\alpha_t = C_\lambda \left\{\frac{k^2}{\varepsilon}(2R) + 3k^{1/2}\left(\frac{\nu^3}{\varepsilon}\right)^{1/4}\frac{(2R)^{1/2}}{Pr} f_d\right\} \times \left\{1-\exp\left(-\frac{y^*}{14}\right)\right\}\left\{1-\exp\left(-\frac{Pr^{1/2}y^*}{14}\right)\right\} \quad (20)$$

and the second is that with $m = 1/2$ (hereinafter referred to as model C):

$$\alpha_t = C_\lambda \left\{\frac{k^2}{\varepsilon}(2R)^{1/2} + 3k^{1/2}\left(\frac{\nu^3}{\varepsilon}\right)^{1/4}\frac{(2R)^{1/2}}{Pr} f_d\right\} \times \left\{1-\exp\left(-\frac{y^*}{14}\right)\right\}\left\{1-\exp\left(-\frac{Pr^{1/2}y^*}{14}\right)\right\}. \quad (21)$$

The prime difference among these three models A–C resides in the representation of the characteristic time scale for turbulent heat transfer in the region away from the wall. Note, however, that models A–C give almost the same thermal field predictions for an equilibrium flow because the time-scale ratio R becomes about 0.5 there. Besides, in proximity to the wall surface, models A–C show exactly the same near-wall limiting behavior, i.e. $\alpha_t \propto \nu_t(R/Pr)^{1/2}$. Thus, all of them can correctly reproduce the near-wall asymptotic relations, regardless of the existence of wall-temperature fluctuations (see ref. [13]).

3.3. *Model constants and model functions*

The model constants and the model functions used in equations (10)–(21) are determined in the following way.

First, C_λ, C_{D1} and C_{D2} are set to 0.1, 2.0 and 0.9, respectively, following the lead of the NTT model [12, 13]. Concerning the turbulent diffusion constants σ_h and σ_ϕ, we assume $\sigma_h \simeq \sigma_k$ and $\sigma_\phi \simeq \sigma_\varepsilon$, and set both of them to the same value of 1.6. The constants C_{P1} and C_{P2} are to be determined with the relation for the 'constant-stress and constant-heat-flux layer' [11–13]:

$$C_{D1} - C_{P1} = 2R\{C_{P2} - C_{D2} + (\kappa^2/Pr_t)/(\sigma_\phi\sqrt{C_\mu})\}. \quad (22)$$

Thus, substituting the standard values of $C_\mu = 0.09$, $R \simeq 0.5$, $Pr_t \simeq 0.9$ and $\kappa \simeq 0.41$ into equation (22), we obtain the optimum values of C_{P1} and C_{P2} after examining the calculated results [see equations (26)–(28)]. The model functions f_{D1} and f_{D2} can be expressed in the same form as in the NTT model [12] by taking account of the wall-limiting behavior:

$$f_{D1} = \left\{1-\exp\left(-\frac{y^*}{A_{D1}}\right)\right\}^2 \quad (23)$$

$$f_{D2} = \left(\frac{1}{C_{D2}}\right)(C_{\varepsilon 2}f_2 - 1)\left\{1-\exp\left(-\frac{y^*}{A_{D2}}\right)\right\}^2 \quad (24)$$

with $f_2 = 1 - 0.3\exp\{-(R_t/6.5)^2\}$, the consequence of equation (9). Here, A_{D1} and A_{D2} are determined after numerical optimization [see equations (25)–(28)]. We put f_{P2} at unity so as to be consistent with the velocity-field model [9], as discussed in the NTT model [12]. In the NTT model [12], f_{P1} is also assumed to be unity. If we set f_{P1} to unity, however, we may encounter computational instability in some kinds of heat-transfer fields where the similarity between the velocity and temperature fields does not exist, as in the experiment of Antonia *et al.* [7]. On the other hand, the model developed by Nagano and Kim [11] does not suffer from any instability, though it uses the model functions of $f_{P1} = f_{D1} = 1.0$. From these facts and some computational attempts, we have concluded that numerical instability can be avoided by setting $f_{P1} \simeq f_{D1}$. Thus, we set $f_{P1} = f_{D1}$ in the present model. Note that the present heat-transfer model with this modification for f_{P1} gives almost the same results as with the NTT model [12] for the fundamental heat-transfer problems, as will be shown later.

In summary, the model constants and the model functions which are commonly used in models A–C are as follows:

$$C_\lambda = 0.1,\ C_{D1} = 2.0,\ C_{D2} = 0.9,$$
$$\sigma_h = 1.6,\ \sigma_\phi = 1.6, \quad (25)$$
$$f_{P1} = f_{D1} = \{1-\exp(-y^*)\}^2$$
$$(\text{i.e. } A_{D1} = 1.0),\ f_{P2} = 1.0.$$

The model constants optimized for each model are as follows:

$$C_{P1} = 1.90,\quad C_{P2} = 0.60,\quad A_{D2} = 5.7 \quad \text{for model A} \quad (26)$$

$$C_{P1} = 1.85,\quad C_{P2} = 0.65,\quad A_{D2} = 5.5 \quad \text{for model B} \quad (27)$$

$$C_{P1} = 1.95,\quad C_{P2} = 0.55,\quad A_{D2} = 5.8 \quad \text{for model C.} \quad (28)$$

Some explanations should be made regarding the dependence of the Prandtl number. The primary subject of the present study is to propose a new heat-transfer model to be applied to separating and reattaching flows. With this in mind, we have only referred to some established discussions on the Prandtl-number dependence [18, 19] in constructing the present heat-transfer model, and restricted the model application only to heat-transfer problems in air ($Pr = 0.71$). To treat the heat transfer at $Pr \gg 1$ or $Pr \ll 1$, the dependence of Pr should be considered in modeling not only the eddy diffusivity for heat but also some model functions. The problem is now under investigation.

4. MODEL ASSESSMENT IN ATTACHED FLOW HEAT TRANSFER

To confirm the basic accuracy of the present heat-transfer models (models A–C), we applied them to two representative turbulent heat-transfer problems in attached flows. The first test case is a boundary-layer heat transfer investigated experimentally by Gibson *et al.* [21], and the second one corresponds with the experiment by Antonia *et al.* [7]. In the first problem [21], the wall surface is heated at a constant wall temperature from the beginning of a boundary-layer development. In the second problem [7], the wall is kept adiabatic in the initial development of a boundary layer, and then suddenly heated with a constant heat flux from a location where the boundary layer has developed to some extent. It should be mentioned that the latter case [7] has been found to be too difficult to simulate accurately with the constant turbulent-Prandtl-number assumption because the analogy between the velocity and temperature fields no longer holds.

The computational procedure used in the present study was the same as that of Hattori *et al.* [22], which was based on a finite-volume method developed by Patankar [23] and Leschziner [24]. The number of grid points across the boundary layer was 201, where the grid points were concentrated in the neighborhood of the wall surface to resolve the viscous sublayer sufficiently and to obtain a grid-independent solution [22]. For the technique to specify the boundary conditions, we followed Youssef *et al.* [13]. The temperature variation on the wall surface was set to zero to meet the measurement conditions.

The calculated mean-velocity and mean-temperature profiles corresponding to Gibson *et al.*'s experiment [21] are shown in Fig. 1. From Fig. 1(a), it can be seen that the present velocity-field model [9] predicts the mean-velocity profile as accurately as the NT model [10]. We can also acknowledge from Fig. 1(b) that all three models A–C give almost the same results in good agreement with the experimental data [21] as the NTT model [12].

The predicted streamwise development of mean-temperature for the second test case (Antonia *et al.* [7]) is shown in Fig. 2, and the relevant development of turbulent heat flux is presented in Fig. 3. The location x in Figs. 2 and 3 indicates the streamwise distance from the beginning point of heating. From these two figures, it can be seen that all three models A–C show good agreement with the experimental data, whereas the conventional prediction with the constant turbulent Prandtl number, $Pr_t = 0.9$, shows a substantial underprediction for the mean-temperature variation.

The foregoing comparisons have proven that the present models can quite accurately predict both the velocity and the temperature fields in attached turbulent flows even with a sudden change of wall thermal conditions.

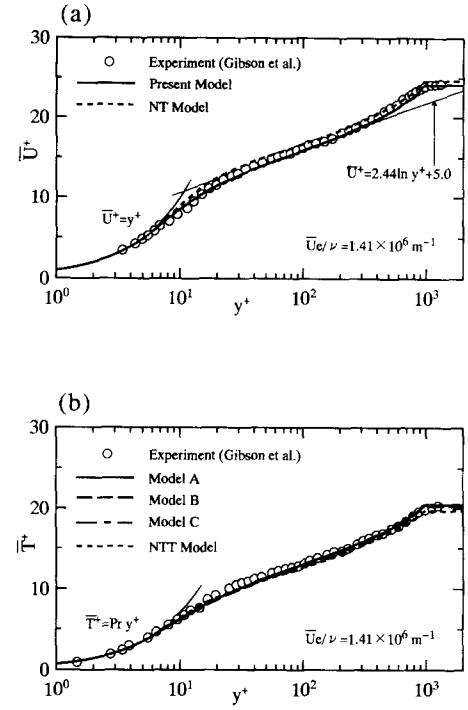

Fig. 1. Comparison with the experiment by Gibson *et al.* in boundary layer: (a) mean velocity; (b) mean temperature.

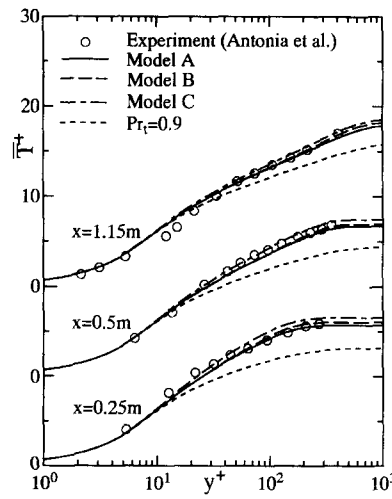

Fig. 2. Streamwise development of mean temperature.

5. APPLICATION TO BACKWARD-FACING STEP FLOWS

5.1. *Model assessment with DNS data on flow field*

As discussed in the preceding paper [9], the accurate prediction of heat transfer in separating flows is impossible without reliable predictions of the flow field in the recirculating region. We have shown that the velocity-field model described in Section 2 predicts backward-facing step flows quite successfully for various flow conditions.

Recently, Le *et al.* [25] performed a direct numerical simulation (DNS) of a backward-facing step flow.

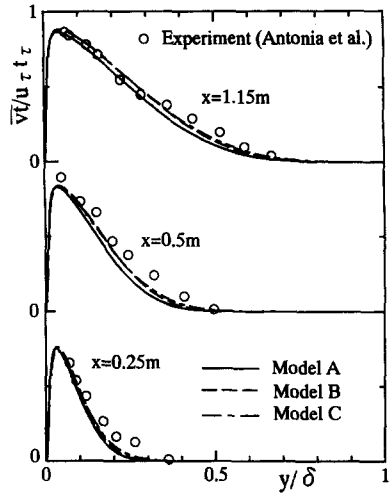

Fig. 3. Streamwise development of turbulent heat flux.

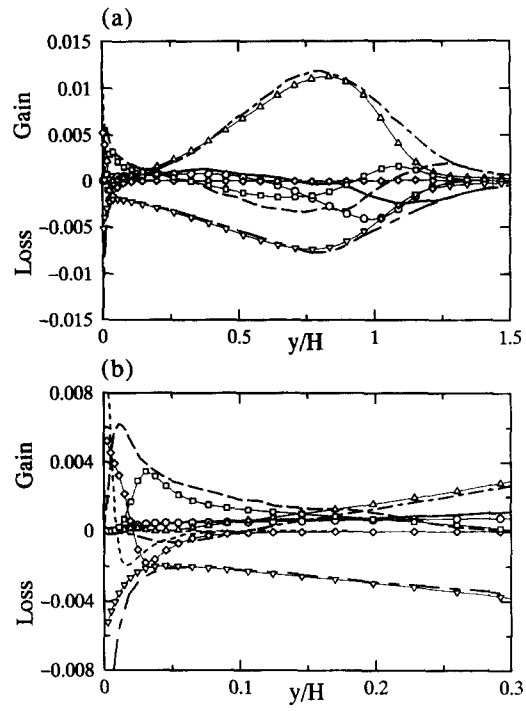

Fig. 4. Budget of turbulent energy at $x/H = 4$ (normalized by $\tilde{U}_0^3/H$): convection ○ model, ——— DNS; turbulent diffusion □ model, — — — DNS; viscous diffusion ◇ model, - - - - - - - DNS; production △ model, — · — · — DNS; dissipation ∇ model, ——— DNS; (a) overall view; (b) close to wall on step side.

DNS data are very useful for modeling a flow with separation. Especially, the turbulence-energy budget close to the wall is the most important knowledge on heat transfer, since the structure of turbulent heat transfer is almost entirely determined there. Therefore, in order to assess the accuracy of the present model for flow field in further detail, we performed the calculation corresponding to the DNS by Le *et al.* [25] and compared the computed results with the DNS data. The computational technique used is the same as that in the preceding paper [9], except that we have adopted here the most recent scheme of Kuno *et al.* [26] for pressure calculation. The essential validity of the numerical procedure was already discussed in ref. [9]. The number of grid points used in this calculation is $N_\xi \times N_\eta = 389 \times 145$, so the grid spacing is sufficiently fine to obtain a grid-independent solution [9]. The Reynolds number is at $Re_H = 5100$, and the channel expansion ratio, ER, is 1.2. The velocity-field profile of a boundary-layer flow at $Re_\theta = 670$ is adopted as the inlet boundary condition, corresponding to the DNS [25].

The present prediction of the flow reattachment length becomes: $X_R/H = 5.92 \pm 0.02$, which agrees well with the DNS value of $X_R/H = 6.0$ [25]. The uncertainty in the predicted reattachment length (± 0.02) is approximately equal to the grid spacing near the reattachment point. The budget of the turbulent energy at $x/H = 4$ in the recirculating region is shown in Fig. 4. From Fig. 4(a), one can see that the present results show excellent agreement with the DNS [25] over the whole region. The production and dissipation terms, which are the leading terms in the budget, are predicted quite accurately, though the convection and the turbulent diffusion terms peak around $y/H \simeq 1$, being slightly closer to the wall than the DNS data. In the proximity of the wall, the computational results are in good agreement with the DNS data as shown in Fig. 4(b), except that the turbulent diffusion shows an underprediction for the DNS data in the limited region very close to the wall. It should be mentioned, however, that the present result gives the correct near-wall tendency of the dissipation rate that a local maximum occurs at the wall. The profile of ε near the wall indicates that the simplified wall-boundary condition, $\partial\varepsilon/\partial n = 0$, has no validity, although it has been occasionally adopted as a temporary expedient.

From the above discussions, it is confirmed that the prediction by the present velocity-field model [9] is sufficiently reliable even in the recirculating region of a backward-facing step flow.

5.2. *Numerical procedure and boundary conditions for thermal field*

In calculating the heat transfer in the backward-facing step flow, the finite-difference method was used to discretize the governing equations (10)–(12). We adopted the third-order upwind difference for the convection term in equation (10), the first-order upwind difference for the convection terms in equations (11) and (12), and the second-order central difference for the other terms. Time integration for the thermal field was performed by the Euler-Implicit method. The computational technique and the turbulence model for the velocity field were the same as in Section 5.1. Figure 5 shows the computational grid system. The generalized coordinate system was employed, where only the pressure was located in a staggered

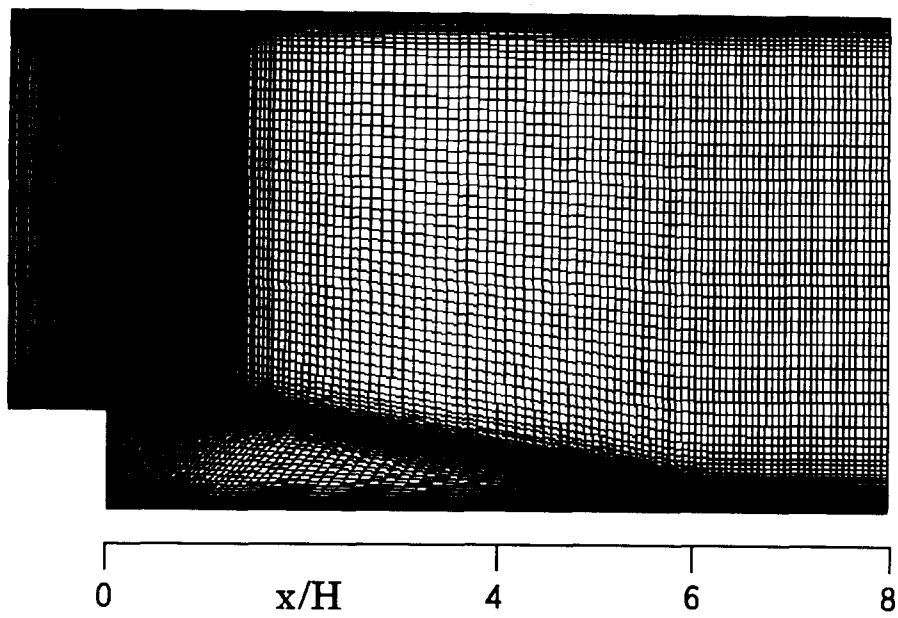

Fig. 5. Grid system (partial view).

position [26]. The computational domain is: $-3.8H \leqslant x \leqslant 50H$. And the number of grid points is: $N_\xi \times N_\eta = 287 \times 125$, which is enough to provide grid-independent solutions for the velocity [9]. Also, these grid points suffice for temperature-field calculations because the thickness of the conductive sublayer in an air flow ($Pr = 0.71$) is generally expected to be almost the same as that of the viscous sublayer.

The calculations were conducted corresponding to the experiment by Vogel and Eaton [27]. The channel expansion ratio is $ER = 1.25$ and the working fluid is air. We computed the thermal field for five variations of the flow conditions, i.e. two cases at different Reynolds numbers, Re_H, and three cases with different upstream boundary-layer thicknesses, δ_0/H, as summarized in Table 1. The boundary conditions for the thermal field are: q_w = constant on the step side wall at $x > 0$, or 0 on the other wall surfaces, $\overline{t^2} = 0$ and $\varepsilon_{tw} = \alpha(\partial\sqrt{\overline{t^2}}/\partial n)^2$ at all wall surfaces; $\bar{T}$ is uniform at the inlet, and $\overline{t^2}$ and ε_{tw} are set at a sufficiently small value of an order 10^{-12} corresponding to experimental perturbations at the inlet; and $\partial^2\bar{T}/\partial x^2 = \partial^2\overline{t^2}/\partial x^2 = \partial^2\varepsilon_t/\partial x^2 = 0$ at the outlet. It should be noted that the present boundary condition for ε_t at the wall surface is identical with the strict one (see Youssef *et al.* [13]).

Table 1. Computational conditions for back-step flows

Case	1	2	3	4	5
Re_H	28 000	28 000	28 000	13 000	13 000
Re_θ	3000	1800	500	2000	1200
δ_0/H	1.1	0.7	0.15	1.1	0.7

6. RESULTS AND DISCUSSION

6.1. *Comparison with experimental data*

The computational results for the velocity field for case 1 in Table 1 are shown in Fig. 6. The predicted flow reattachment length is $X_R/H = 6.69 \pm 0.04$, which is in excellent agreement with the experimental result, $X_R/H \simeq 6.67$ [27]. The distributions of mean velocity and skin friction coefficient are successfully simulated as shown in Fig. 6(b) and (c), though the skin friction coefficient in the recirculating region is slightly overpredicted compared with the experimental data.

The computational results for the thermal field in case 1 are shown in Fig. 7. From Fig. 7(a), we can recognize that the predictions of the Stanton number with all three models A–C are in good agreement with the experimental data [27], whereas the conventional calculation with $Pr_t = 0.9$ gives substantial overpredictions by as high as 30%. The maximum Stanton numbers predicted by the models A–C are located in the region slightly upstream of the flow reattachment point, which agrees completely with the experimental finding by Vogel and Eaton [27]. Investigating the computational results of three models A–C in detail, we see that model A shows the best agreement with the experiment, and the position of the maximum Stanton number predicted with model B is located slightly more upstream than with the other two models.

The predicted mean-temperature profiles, on the other hand, exhibit different tendencies among the models as shown in Fig. 7(b). The variation of mean temperature around a location equal to the step height ($y/H \simeq 1$) is very important to examine the validity of the characteristic time scale used for modeling turbulent heat transfer. From Fig. 7(b), we notice that

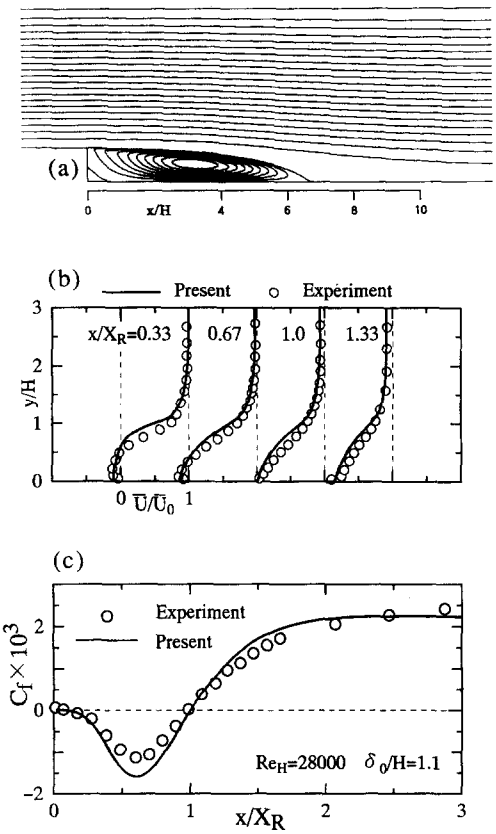

Fig. 6. Computational results for velocity field (case 1): (a) streamlines; (b) mean streamwise velocity; (c) skin friction coefficient.

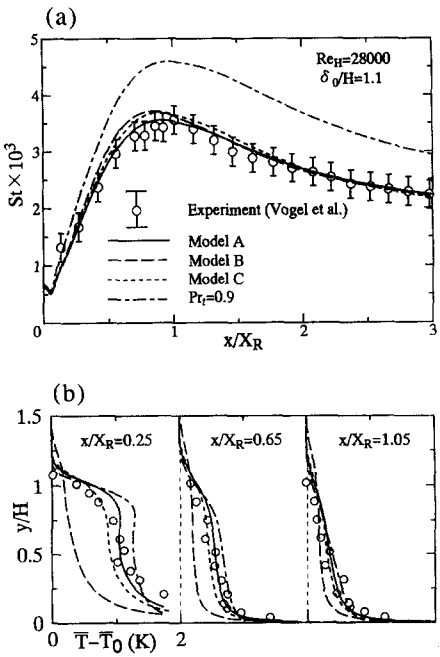

Fig. 7. Comparison with Vogel *et al.*'s experiment (case 1): (a) Stanton number on step side wall; (b) mean temperature [key as (a)].

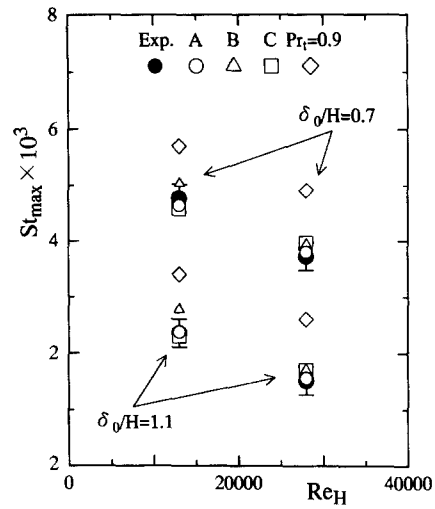

Fig. 8. Variation of maximum Stanton number.

model B gives a tendency different from the experimental data [27]; the others show reasonable variations with a marked kink around the step-height location ($y/H \simeq 1$), and the mean temperature profiles are in good overall agreement with the experiment. The maximum Stanton numbers obtained from the computational results for cases 1, 2, 4 and 5 are summarized in Fig. 8, from which we can readily see that the Reynolds-number dependence of the maximum Stanton number differs with models. When the upstream boundary-layer thickness δ_0 is fixed, model B shows the greatest Reynolds-number dependence of the maximum Stanton number. Model A indicates a Re_H-dependence greater than do model C and the constant-Pr_t calculation. The Re_H-dependence predicted by model C and the constant-Pr_t calculation are found to be similar to that in a flat-plate flow, which conflicts with the experimental evidence [1, 27]. From Fig. 8, one can eventually see that model A gives the best agreement with the experimental data on maximum Stanton numbers.

As a result of these discussions, we have concluded that model A is the most appropriate model to calculate accurately the turbulent heat transfer in complex flows with separation and reattachment. In what follows, we discuss in more detail the turbulent heat transfer in backward-facing step flows through the computational results obtained from model A.

6.2. *Confusions in previous predictions*

First of all, we compare our computational results with those by previous representative k–ε models to confirm the accuracy of our model performance and to investigate the relation between the velocity and temperature fields for turbulent heat transfer in a separated and reattaching flow. The Launder–Sharma model (hereinafter referred to as the LS model) [28] and that with the Yap correction (referred to as the LS+Yap model) [1] are selected for comparison because the former was the first low-Reynolds-num-

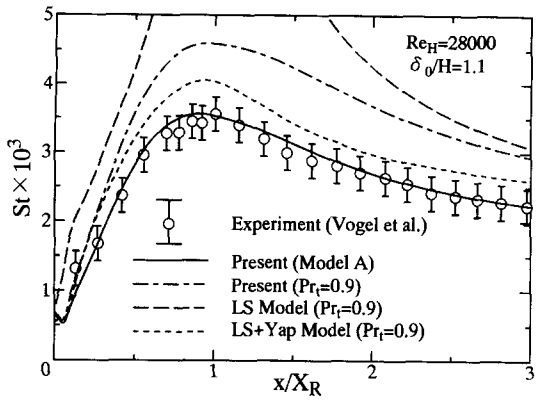

Fig. 9. Comparison of model results for Stanton number (case 1).

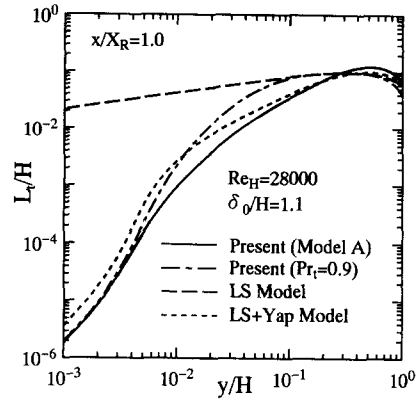

Fig. 10. Comparison of length scale for turbulent heat transfer (case 1).

ber k–ε model applied to the calculations of turbulent heat transfer with flow separation and reattachment, while the latter has been most commonly adopted in thermal-field calculations in the near-wall region of separating and reattaching flows [1].

The comparison of the calculated Stanton numbers for case 1 is shown in Fig. 9. Launder *et al.* [1, 28] demonstrated that the heat-transfer coefficients predicted with the LS model were about five times too high in the vicinity of the maximum heat-transfer point, as compared with the experimental data. This was due to the relatively small thickness of the viscous (conductive) sublayer and to the calculated too much larger turbulent length scales. Thus, it has been long believed that the low-Reynolds-number form of the k–ε model is not suited for heat-transfer calculation in a separated and reattaching flow. Figure 9 reconfirms that the LS model gives the same trend as in the previous studies [1, 28], in which the Stanton numbers were surprisingly overpredicted. The Yap correction [1] is regarded as a powerful measure to reduce the near-wall turbulent length scale in a separated flow, in particular near the flow reattachment point around which the maximum heat transfer occurs. From Fig. 9, we recognize that while the Yap correction offers remarkable improvements over the original LS model, it still suffers from overpredictions. On the other hand, the prediction with model A definitely gives the best agreement with the experimental data.

The comparison of the turbulent length scales for heat transfer at the flow reattachment point, $L_t = \alpha_t/k^{1/2}$, obtained from the computational results is shown in Fig. 10. Note that the difference in length scale between model A and the constant-Pr_t calculation in Fig. 10 is due to the difference of the characteristic time scale, although they use completely the same velocity-field data. From Fig. 10, we can see that the proposed model gives the proper turbulent length scale near the wall and the order of the magnitude of calculated Stanton numbers in Fig. 9 is proportional to that of the length scales in the near-wall region of $0.02 \leqslant y/H \leqslant 0.04$, where the eddy diffusivity for heat dominates over the molecular diffusivity.

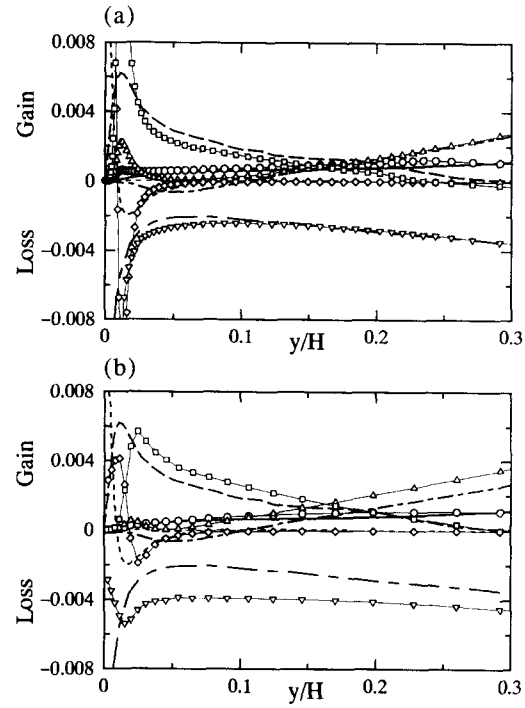

Fig. 11. Budget of turbulent energy close to wall at $x/H = 4$ (key as Fig. 4): (a) original Launder–Sharma model; (b) Launder–Sharma model with Yap correction.

As discussed before, in order to extend the applicability of the heat-transfer model to complex flows with separation and reattachment, accurate prediction of the turbulent velocity field in the near-wall region is indispensable. Thus, to examine the accuracy of the turbulence models in the near-wall region of separated flows, calculations with the LS and the LS+Yap models, corresponding to the DNS by Le *et al.* [25], were performed. Comparisons of the turbulent-energy budget with the DNS data are shown in Fig. 11. Two points should be mentioned with regard to this figure. First, in the near-wall region $y/H \leqslant 0.05$, most of the predicted terms with the LS model show an unacceptable overestimation in comparison with the DNS data as shown in Fig. 11(a). In particular, the model

predictions of the turbulent diffusion, the viscous diffusion and the total dissipation rate are more than twice as large as the DNS data. Note that, in these models, the total dissipation rate is expressed as follows:

$$\varepsilon_{\text{total}} = \varepsilon + 2\nu\left(\frac{\partial\sqrt{k}}{\partial y}\right)^2. \tag{29}$$

Figure 11(a) also shows that the spiky behavior of the production term appears in the immediate vicinity of the wall but not in the DNS data. These enormous overpredictions and unexpected variations are thought to be the main reason why the original LS model overpredicts the heat-transfer coefficient in the recirculating region. Secondly, it is surprising that the LS+Yap model does not accurately reproduce the turbulent-energy budget of the DNS data as shown in Fig. 11(b). The prediction of the distribution of the total dissipation rate is worse than by the original one in the region $y/H \geqslant 0.05$. Moreover, in close proximity to the wall, the viscous diffusion and the total dissipation terms have the respective local peak values around $y/H \simeq 0.02$. This conflicts with the DNS data, according to which each local peak appears just at the wall. Again, it should be emphasized that the dissipation rate predicted by the present velocity-field model shows the correct behavior in the proximity of the wall and agrees almost perfectly with the DNS data in the region $y/H \geqslant 0.05$, without any additional amendment term (see Fig. 4).

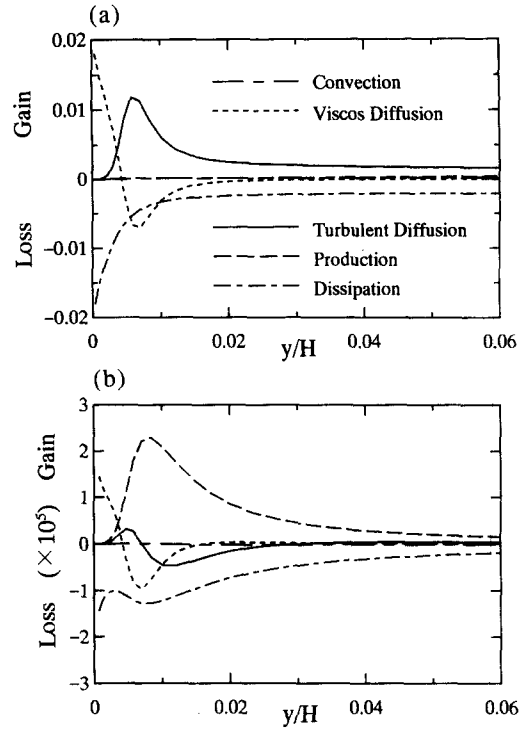

Fig. 12. Comparison of budget close to wall at reattachment point (case 1, model A): (a) turbulent energy (normalized by $\bar{U}_0^3/H$); (b) temperature variance [normalized by $\bar{T}_r^2\bar{U}_0/H$, key as (a)].

6.3. *Thermal field in backward-facing step flow*

Comparisons of the budgets of both the turbulent energy k and the temperature variance $\overline{t^2}$ close to the wall at the reattachment point in case 1 are shown in Fig. 12. As shown in Fig. 12(a), the production term of the turbulent energy equation is negligibly small near the reattachment point because the mean shear of the velocity $\partial\bar{U}/\partial y$ almost vanishes there. As a result, in this region, the turbulent diffusion term dominates the gain side of the budget. Such a turbulence energy balance is never seen in an ordinary attached shear flow. On the other hand, the budget of the temperature variance essentially remains similar to that in a flat-plate or channel flow [20] because the temperature field with heat input from the wall has the substantial mean temperature gradient $\partial\bar{T}/\partial y$ even in the recirculating-flow region. Therefore, in the thermal field, the main term on the gain side is the production term. As a consequence, no similarity exists between the velocity and the temperature fields in this type of heat-transfer situation.

Here, the question arises: Can one accurately predict the turbulent heat transfer in separating flows with the constant-Pr_t model, if accurate velocity-field data are given? As shown previously, accurate prediction for a suddenly-heated flow is impossible with the constant-Pr_t model. In that case, there also exists dissimilarity between the velocity and temperature fields. On the other hand, reasonable predictions can be achieved with the two-equation heat-transfer model as shown in Figs. 2 and 3. Figure 13 shows the turbulent-Prandtl-number distributions in the suddenly-heated flow corresponding to Antonia *et al.*'s experiment [7] and in the backward-facing step flow for case 1, both of which are computed using model A. The calculated turbulent Prandtl numbers in both cases are much higher than the conventional value of $Pr_t = 0.9$ and, of course, not constant. The present results for the former case agree with the experimental fact indicated by Sato *et al.* [8]. From Fig. 13(b), the Yap correction mentioned before seems to be too effective in reducing the turbulent length scale by substantially overestimating the total dissipation rate, though it leads to a reasonable heat-transfer coefficient with $Pr_t = 0.9$. The internal inconsistency, however, cannot be avoided, and the significant departure from the DNS data on the energy balance shown in Fig. 11(b) is a salient example.

The mean temperature profiles normalized by the wall parameters for case 1 are shown in Fig. 14, and the distributions of temperature variance and turbulent heat flux in Fig. 15. Corresponding profiles for the 'Boundary Layer,' obtained with model A for the experiment by Gibson *et al.* [21], are shown in these figures for comparison. From Fig. 14, it can be seen that the computed temperature profiles lie considerably lower than in the boundary layer, in agree-

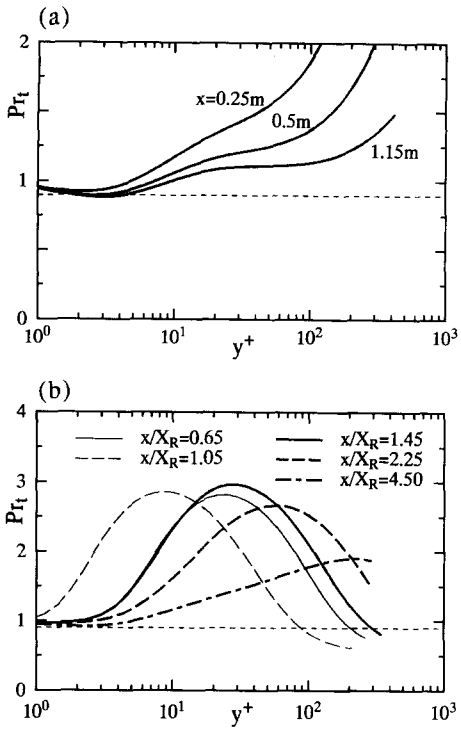

Fig. 13. Variation of turbulent Prandtl number (model A): (a) suddenly heated boundary layer; (b) backward-facing step flow (case 1).

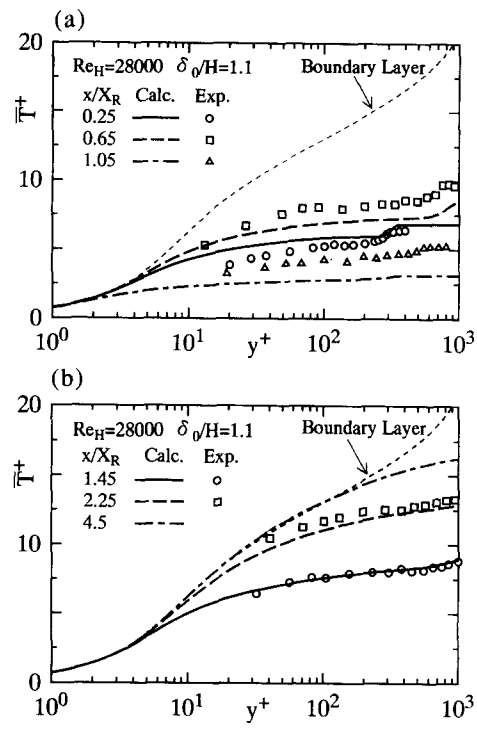

Fig. 14. Mean temperature profiles normalized by wall parameters (case 1, model A): (a) recirculating region; (b) redeveloping region.

ment with the experimental data† [27]. This tendency of the temperature profile appears to be essentially similar to that of the velocity field as discussed in the earlier paper [9, 29]. Figure 15 indicates the characteristics of the turbulent heat transfer in separating flows. Obviously, the near-wall profiles of scalar turbulence are completely different from the familiar shapes in a boundary layer. From these results, we may conclude that the conventional log-law is inapplicable not only to the velocity but also to the temperature in a separated and reattaching flow.

6.4. *Influence of upstream boundary-layer thickness on heat transfer*

The effect of the upstream boundary-layer thickness on the Stanton number distribution is shown in Fig. 16, from which we can ascertain that the present model reproduces the characteristics of the Stanton number, according to which a peak value increases as the upstream boundary-layer thicknesses decrease. It should be emphasized that this quantitative agreement has never been achieved with any previous turbulence models to date [2]. The streamwise variations of the local maximums of eddy viscosity ν_t, and cross-

† The friction temperature is expressed as $t_\tau = (q_w/\rho c_p u_\tau) = (q_w/\rho c_p \bar{U}_0)/(u_\tau/\bar{U}_0)$. In calculating t_τ from the experimental data, a value of $q_w/\rho c_p \bar{U}_0$ is obtained from the wall temperature (ref. [27], Fig. 9) and the Stanton number (ref. [27], Fig. 12). On the other hand, a value of $u_\tau/\bar{U}_0$ is obtained from the distribution of mean skin friction coefficient (ref. [27], Fig. 10).

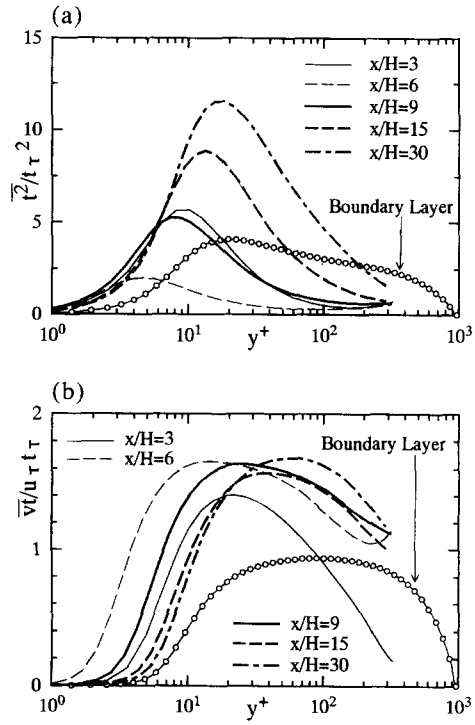

Fig. 15. Distributions of turbulent heat transfer characteristics (case 1, model A): (a) temperature variance; (b) turbulent heat flux.

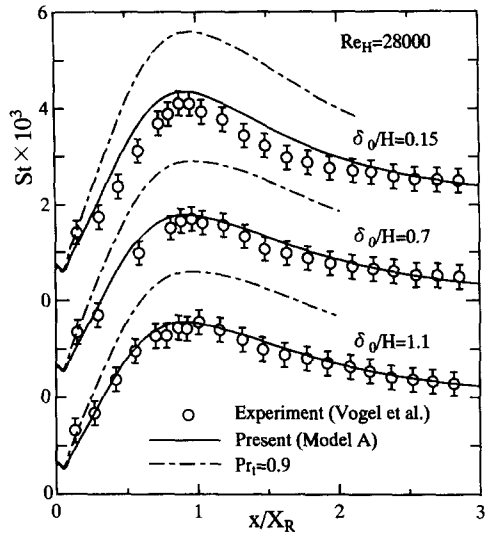

Fig. 16. Effect of upstream boundary-layer thickness on Stanton number (model A).

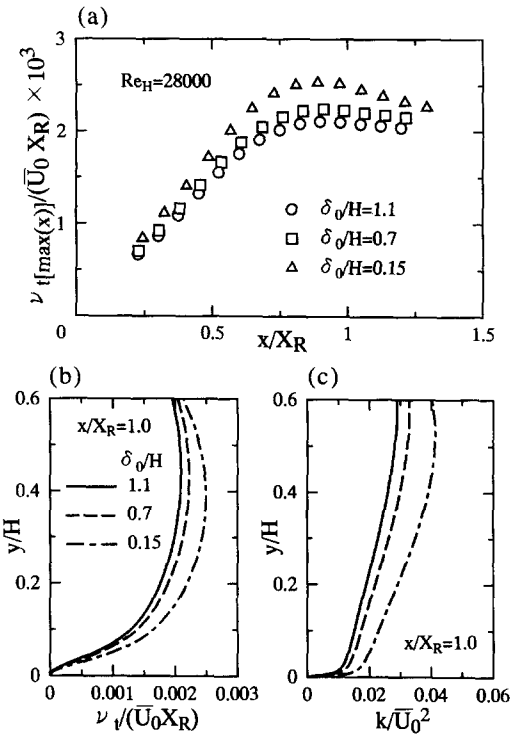

Fig. 17. Effect of upstream boundary-layer thickness on turbulence characteristics ($Re_H = 28\,000$): (a) streamwise variation of local maximum values of eddy viscosity; (b) cross-streamwise variation of eddy viscosity; (c) cross-streamwise variation of turbulent energy [key as (b)].

streamwise variations of eddy viscosity ν_t and turbulent energy k at the reattachment point for cases 1–3 are shown in Fig. 17. Streamwise variations of the local ν_t maximums show a common tendency: the local maximum increases linearly with the distance from the separation point and peaks at a location slightly upstream of the reattachment point. The maximum values range from 0.002 to 0.0025 as shown in Fig. 17(a), consistent with the results in the earlier paper [9]. Moreover, the present investigation has elucidated that a slight difference in the growth rate of eddy viscosity greatly influences the heat-transfer rate. As pointed out by Vogel and Eaton [27] and Adams and Eaton [30], the shear-layer turbulence increases with a decrease of the upstream boundary-layer thickness. Accordingly, the eddy viscosity in the shear-layer can be expected to increase with the decrease in upstream boundary-layer thicknesses, as seen in Fig. 17(a). Further, we notice that the effect of the initial boundary-layer thickness on the turbulence quantities in the shear-layer region is maintained well into the region very close to the wall surface, as shown in Fig. 17(b) and (c). Thus, the streamwise variations of the turbulence quantities (e.g. k and ν_t) in the near-wall region are greatly affected by the corresponding variations in the separated shear layer.

On the other hand, as suggested by Vogel and Eaton [27], the streamwise variation of the fluctuating skin friction coefficient C_f' is very similar to that of the heat-transfer coefficient. As discussed in the preceding paper [9], C_f' is closely related to the dissipation rate on the wall ε_w, which can be expressed as follows:

$$C_f' = \frac{\rho\{(b_{11}+\frac{1}{3})\nu\varepsilon_w\}^{1/2}}{\frac{1}{2}\rho\bar{U}_0^2} \tag{30}$$

where b_{11} is the streamwise anisotropy tensor. Needless to say, the dissipation rate in the vicinity of the wall is closely related to the turbulent energy there, so the streamwise variation of C_f' is expected to follow the turbulent energy (or eddy viscosity) variation shown in Fig. 17. The fluctuating skin friction and heat-transfer coefficients are shown in Fig. 18, where C_f' is obtained from equation (30) with the assumption that $b_{11} \simeq 0.5$, based on the channel flow data. The predicted distributions of the fluctuating skin friction coefficient show a reasonable coincidence with the experimental data of Vogel and Eaton [27] as shown in Fig. 18(a), though the calculations follow curves a little higher than do the experiments. However, as mentioned in our earlier study [9], Kasagi *et al.* [31] indicated experimentally that b_{11} can become smaller than b_{33} near the reattachment point, so the actual level of the calculated C_f' can thus be lower than that in Fig. 18(a), leading to better agreement with the experimental data. It is also seen from Fig. 18 that the present computations support the experimental conclusion by Vogel and Eaton [27] that the variation of fluctuating skin friction coefficient C_f' is very similar to that of heat-transfer coefficient.

From these discussions, it can be concluded that the heat-transfer coefficient strongly depends on the near-wall turbulence intensity dominated essentially by the variation of turbulent energy (or eddy viscosity) in the separated shear layer near the reattachment point. This causal sequence, one must conclude, is the main reason why the maximum heat-transfer coefficient increases with the decrease in upstream boundary-layer thicknesses.

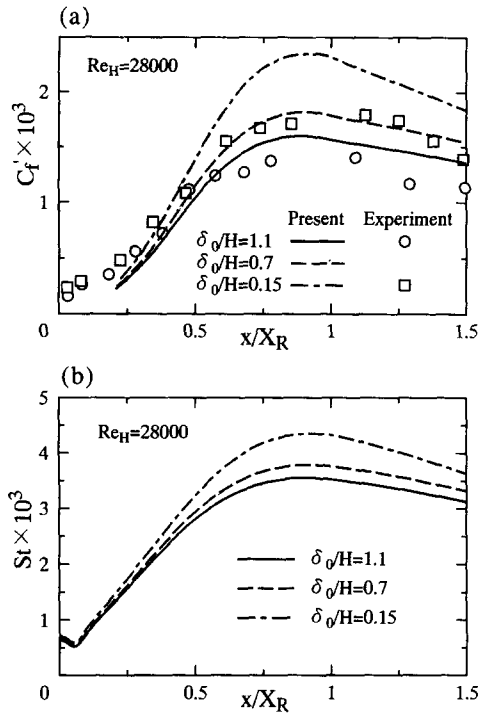

Fig. 18. Comparison of streamwise variation of fluctuating skin friction coefficient and Stanton number on step side wall (Re_H = 28 000, model A): (a) fluctuating skin friction coefficient; (b) Stanton number on step side wall.

7. CONCLUDING REMARKS

We have proposed an improved low-Reynolds-number two-equation heat-transfer model where $u_\varepsilon = (\nu\varepsilon)^{1/4}$ is introduced as the characteristic velocity to account for the near-wall and low-Reynolds-number effects. We have also examined the characteristic time scale for turbulent heat transfer and have found that a composite time scale which gives weight to a shorter scale among the velocity- and temperature-field time scales is the most appropriate.

It is shown that the proposed model predicts quite successfully the heat transfer in an attached boundary-layer flow subjected to a sudden change of the wall-heating condition and in a separating and re-attaching flow downstream of a backward-facing step. Especially, the calculated Stanton numbers in backward-facing step flows are in excellent agreement with the experimental data of Vogel and Eaton [27] under various conditions of the Reynolds number and the upstream boundary-layer thickness.

Our computational results of fluid flow and related heat transfer downstream of a backward-facing step reveal the following: (1) In the flow reattachment zone, the turbulent-energy balance is totally different from that in a boundary-layer flow. The budget of temperature variance, on the other hand, remains similar to that in a boundary-layer flow, at least qualitatively. (2) In the recirculating region, the turbulent Prandtl number has a value substantially higher than the standard one of $Pr_t = 0.9$. Such phenomena can also be seen in some classes of attached flows subjected to a sudden change of wall thermal conditions, and thus should be regarded as a natural consequence of dissimilarity between the velocity and temperature fields. (3) The conventional log-laws for not only the velocity but also the temperature cannot be applied to complex flows with separation.

Finally, we emphasize again that the accurate prediction of heat transfer in separating flows is impossible without reliable predictions of the flow field in the vicinity of the wall in the recirculating region. Thus, it is indispensable to use a low-Reynolds-number turbulence model which can fully resolve the near-wall region. Once the velocity field is obtained with high accuracy, the two-equation heat-transfer model is particularly appropriate for predicting heat transfer in separating flows where the similarity between the velocity and temperature fields fails entirely.

From these arguments, the proposed two-equation heat-transfer model (model A) is considered highly effective for analyzing complex heat-transfer problems involving flow separation and reattachment.

REFERENCES

1. B. E. Launder, On the computation of convective heat transfer in complex turbulent flows, *J. Heat Transfer* **110,** 1112–1128 (1988).
2. M. Ciofalo and M. W. Collins, k–ε predictions of heat transfer in turbulent recirculating flows using an improved wall treatment, *Numer. Heat Transfer* **B 15,** 21–47 (1989).
3. S. Dutta and S. Acharya, Heat transfer and flow past a backstep with the non linear k–ε turbulence model and the modified k–ε turbulence model, *Numer. Heat Transfer* **A 23,** 281–301 (1993).
4. S. Nešić and J. Postlethwaite, Calculation of wall-mass transfer rates in separated aqueous flow using a low Reynolds number k–ε model, *Int. J. Heat Mass Transfer* **35,** 1977–1985 (1992).
5. C. G. Speziale, Analytical methods for the development of Reynolds stress closures in turbulence, *Ann. Rev. Fluid Mech.* **23,** 107–157 (1991).
6. S. Thangam and C. G. Speziale, Turbulent flow past a backward-facing step: a critical evaluation of two-equation models, *AIAA J.* **30,** 1314–1320 (1992).
7. R. A. Antonia, H. Q. Danh and A. Prabhu, Response of a turbulent boundary layer to a step change in surface heat flux, *J. Fluid Mech.* **80,** 153–177 (1977).
8. H. Sato, Y. Nagano and M. Tagawa, Distributions of turbulence quantities and their production, diffusion and dissipation in the thermal entrance region of a pipe, *JSME J.* **B 58,** 2840–2847 (1992).
9. K. Abe, T. Kondoh and Y. Nagano, A new turbulence model for predicting fluid flow and heat transfer in separating and reattaching flows—I. Flow field calculations, *Int. J. Heat Mass Transfer* **37,** 139–151 (1994).
10. Y. Nagano and M. Tagawa, An improved k–ε model for boundary layer flows, *J. Fluids Engng* **112,** 33–39 (1990).
11. Y. Nagano and C. Kim, A two-equation model for heat transport in wall turbulent shear flows, *J. Heat Transfer* **110,** 583–589 (1988).
12. Y. Nagano, M. Tagawa and T. Tsuji, An improved two-equation heat transfer model for wall turbulent shear flows, *Proc. ASME/JSME Thermal Engineering Joint Conference* (Edited by J. Lloyd and Y. Kurosaki), Vol. 3, pp. 233–240 (1991).
13. M. S. Youssef, Y. Nagano and M. Tagawa, A two-

equation heat transfer model for predicting turbulent thermal fields under arbitrary wall thermal conditions, *Int. J. Heat Mass Transfer* **35,** 3095–3104 (1992).
14. H. K. Myong and N. Kasagi, A new approach to the improvement of k–ε turbulence model for wall-bounded shear flows, *Int. J. Japan Soc. Mech Engrs Ser.* II **33,** 67–72 (1990).
15. T. P. Sommer, R. M. C. So and H. S. Zhang, Near-wall variable-Prandtl-number turbulence model for compressible flows, *AIAA J.* **31,** 27–35 (1993).
16. S. E. Elghobashi and B. E. Launder, Turbulent time scales and the dissipation rate of temperature variance in the thermal mixing layer, *Phys. Fluids* **26,** 2415–2419 (1983).
17. O. Zeman and J. L. Lumley, Modeling buoyancy driven mixed layers, *J. Atmos. Sci.* **33,** 1974–1988 (1976).
18. N. Shikazono and N. Kasagi, Modeling Prandtl number influence on scalar transport in isotropic and sheared turbulence, *Proceedings of 9th Symposium on Turbulent Shear Flows*, pp. 18.3.1–18.3.6 (1993).
19. T. Cebeci, A model for eddy conductivity and turbulent Prandtl number, *J. Heat Transfer* **95,** 227–234 (1973).
20. N. Kasagi, Y. Tomita and A. Kuroda, Direct numerical simulation of passive scalar field in a turbulent channel flow, *J. Heat Transfer* **114,** 598–606 (1992).
21. M. M. Gibson, C. A. Verriopoulos and Y. Nagano, Measurements in the heated turbulent boundary layer on a mildly curved convex surface. In *Turbulent Shear Flows* 3 (Edited by L. J. S. Bradbury *et al.*), pp. 80–89. Springer, Berlin (1982).
22. H. Hattori, Y. Nagano and M. Tagawa, Analysis of turbulent heat transfer under various thermal conditions with two-equation models. In *Engineering Turbulence Modelling and Experiments* 2 (Edited by W. Rodi and F. Martelli), pp. 43–52 (1993).
23. S. V. Patankar, *Numerical Heat Transfer and Fluid Flow*. McGraw-Hill, New York (1980).
24. M. A. Leschziner, An introduction and guide to the computer code PASSABLE, UMIST, Manchester (1982).
25. H. Le, P. Moin and J. Kim, Direct numerical simulation of turbulent flow over a backward-facing step, *Proceedings of 9th Symposium on Turbulent Shear Flows*, pp. 13.2.1–13.2.5 (1993).
26. T. Kuno, N. Satofuka and H. Tokunaga, Numerical solution of incompressible flow of power-law fluid using boundary-fitted curvilinear coordinates, *JSME J.* **B 58,** 2442–2448 (1992).
27. J. C. Vogel and J. K. Eaton, Combined heat transfer and fluid dynamic measurements downstream of a backward-facing step, *J. Heat Transfer* **107,** 922–929 (1985).
28. C. C. Chieng and B. E. Launder, On the calculation of turbulent heat transport downstream from an abrupt pipe expansion, *Numer. Heat Transfer* **3,** 189–207 (1980).
29. E. W. Adams and J. P. Johnston, Flow structure in the near-wall zone of a turbulent separated flow, *AIAA J.* **26,** 932–939 (1988).
30. E. W. Adams and J. K. Eaton, An LDA study of the backward-facing step flow, including the effects of velocity bias, *J. Fluids Engng* **110,** 275–282 (1988).
31. N. Kasagi, A. Matsunaga and S. Kawara, Turbulence measurement in a separated and reattaching flow over a backward-facing step with the aid of three-dimensional particle tracking velocimetry, *J. Wind Engng Ind. Aerodyn.* **46 & 47,** 821–829 (1993).